Journal of Thermal Analysis and Calorimetry (2022) 147:8841–8854
https://doi.org/10.1007/s10973-021-11142-1

Experimental evaluation of the thermal performance and capillary limit of a screen mesh heat pipe using SDBS and Al_2O_3-water-based nanofluids

Anderson Gallego[1] · **Karen Cacua**[2] · **Bernardo Herrera**[2]

Received: 5 July 2021 / Accepted: 1 November 2021 / Published online: 11 January 2022

Abstract

This study evaluates the effect of using alumina (Al_2O_3)-water nanofluids stabilized by sodium dodecylbenzene sulfonate (SDBS) on the thermal performance and capillary limit of a screen mesh heat pipe. Nanofluids were prepared using three Al_2O_3 concentrations (0.1 mass/%, 0.5 mass/%, and 1.0 mass/%) and two SDBS concentrations (0.064 mass/% and 0.32 mass/%). The stability of the nanofluids was studied by means of UV-absorbance measurements prior to the experimental test. The results show that the thermal resistance of the heat pipe decreased by up to 50% with Al_2O_3 and SDBS at concentrations of 0.5 mass/% and 0.32 mass/%, respectively. Nevertheless, the capillary limit was reduced between 25 and 45 W compared to the operation with water. Finally, the capillary limit was improved by 5 W (compared to water) using an Al_2O_3 concentration of 0.1 mass/% and no surfactant.

Keywords Heat pipe · Nanofluids · Capillary limit · Thermal performance · Thermal resistance · Surface tension

List of Symbols

A_e	Evaporator's heat transfer area (m^2)
d	Wire diameter (m)
e	Mesh thickness (m)
h	Heat pipe height (m)
h_e	Heat transfer coefficient (W $m^{-2}K$)
k	Permeability (m^2)
N	Number of screen mesh openings per lineal meter (m^{-1})
Q_{in}	Heat input (W)
R	Thermal resistance (°C W^{-1})
r_v	Vapor-core radius (m)
$\bar{T}_c$	Average condenser temperature (°C)
$\bar{T}_e$	Average evaporator temperature (°C)
T_v	Saturated vapor temperature (°C)
V_c	Mesh volume (m^3)
$V_{t,c}$	Overall volume of the voids in the mesh (m^3)

Greek letters

ϕ_{in}	Inner diameter of the heat pipe
ΔT_e	Temperature difference in the evaporator
ε	Porosity of the wick

Subscripts

c	Condenser
e	Evaporator
v	Vapor

Abbreviations

AFM	Atomic force microscopy
Al_2O_3	Aluminum oxide
Cu	Copper
CuO	Copper oxide
DC	Direct current
DI	Deionized
FE-SEM	Field emission scanning electron microscopy
HTC	Heat transfer coefficient
MgO	Magnesium oxide
NCG	Non-condensable gas
SDBS	Sodium dodecylbenzene sulfonate
TiO_2	Titanium dioxide

✉ Anderson Gallego
anderson.gallego@pascualbravo.edu.co

[1] Research and Innovation in Energy Group (GIIEN), Institución Universitaria Pascual Bravo, Calle 73 No 73a-226, Medellín, Colombia

[2] Advanced Materials and Energy Group, Instituto Tecnológico Metropolitano, Calle 54A No. 30 – 01, Medellín, Colombia

Introduction

Heat pipes are widely used to enhance thermal energy recovery and utilization [1–3], because their heat transfer rates are higher than those of energy transport systems. Said heat pipes take advantage of the latent heat transfer of vaporization at low temperature gradients [4]. Additionally, they operate under the principle of evaporation and condensation of a working fluid, whose liquid phase flows by capillary pumping through a porous medium [5]. Heat pipes have been widely implemented in different engineering devices, mainly electronic systems and heat exchangers, due to their constructive flexibility and outstanding thermal performance [6, 7].

Nevertheless, the behavior of heat pipes depends on the thermo-physical properties of the working fluid, the use of capillary material, operating conditions, and geometric arrangements, which determine their thermal performance and operating limits [8]. Such limits constrain their maximum heat transfer rate and cause failures in their operation. One of the most common operating limits of heat pipes is the capillary limit, which refers to the heat flux in the evaporator at which the capillary pumping capacity of the porous medium is lower than the pressure drops of the liquid and the vapor. In the evaporator, the liquid–vapor interface disappears, causing a temperature rise [9] that, in turn, results in a deterioration of the thermal performance by the increase in thermal resistance of the heat pipe, which stops operating [10]. Therefore, efforts have been made to produce heat pipes with superior capillary limits and thermal performance.

A common method to increase the thermal performance and capillary limit of heat pipes is to use of nanofluids [11, 12], which are colloidal suspensions of solid nanoparticles in a base fluid [13] that enhance the thermal properties of conventional fluids [14, 15]. Some researchers have focused on the experimental and theoretical determination of the effect nanofluids have on capillary limit and thermal performance. For instance, Poplaski et al. [4], and Brahim and Jemni [16], in their numerical study, demonstrated that the thermal resistance of a heat pipe in a horizontal position could be reduced up to 79% using Al_2O_3-, CuO-, and TiO_2-based nanofluids. Furthermore, the utilization of nanoparticles in the working fluid increased the capillary limit.

Hassan and Harmand [17], Kamyar et al. [18], and Putra et al. [19] experimentally achieved a superior thermal performance using Cu, CuO, and Al_2O_3 nanofluids. They managed to decrease the thermal resistance by up to 65% in the case of Al_2O_3 nanofluids and attributed the reduction in thermal resistance to the fact that nanoparticles tend to float on vapor bubbles during their formation. As a result, the nucleation size of vapor bubbles is smaller, and the thermal resistance of the heat pipes is lower than when the working fluid does not contain nanoparticles. Other authors such as Ghanbarpour et at. [20, 21] have attributed the improvement in thermal performance and capillary limit to the deposition of nanoparticles on the mesh and heat transfer surface in the evaporator section, which increases the heat transfer area and the capillary pumping capacity. They established that the thermal resistance decreased as the concentration of nanoparticles increased. Similarly, Kim and Bang [9] investigated the effect of using graphene oxide nanofluids. They found that the capillary limit increases with nanofluids compared to DI-water since nanoparticles deposited on the mesh enhanced the wettability and capillary radius; consequently, the capillary pumping was increased, and the thermal resistance was reduced by 25%. Nevertheless, although Kim et al. [22] also found that the deposition of nanoparticles on the mesh enhanced wettability and capillarity, in their case, the thermal resistance increased as well as the concentration of nanoparticles increased.

In general, thermal performance and capillary limit parameters can be improved using nanofluids because they produce phenomena such as increased wettability, changes in surface tension and heat transfer surface, and nanoparticle deposition. However, the use of nanofluids also presents limitations that include stability because nanoparticles are in constant Brownian motion and subject to van der Waals forces that promote their agglomeration and sedimentation [23–25]. This poses problems when nanofluids are employed in heat pipes because large agglomerates can cause a clogging of the pores of the capillary material and generate additional thermal resistance [26, 27]. Therefore, multiple dispersion methods have been used; for instance, the addition of chemical agents such as surfactants, which may increase the dispersion of nanoparticles in base fluids [28].

Menlik et al. [29] investigated the effect of MgO-water nanofluids on the thermal performance of a wickless heat pipe using Triton X-100 as surfactant. They found that the thermal performance was increased by 26% at a power input of 200 W. Additionally, Sözen et al. [30] obtained an increase in the thermal performance of a wickless heat pipe using fly-ash and Al_2O_3 nanofluids and Triton X-100 as the dispersion method. The thermal resistance was reduced by 30.1% with fly-ash nanofluids and by 5.2% with Al_2O_3 nanoparticles in concentrations of 2.0 mass/%.

The effect of surfactants on the capillary limit and thermal performance of heat pipes has been studied superficially, but several authors indicate that they contribute to stability and increased wettability due to a reduction in surface tension. As a consequence, surfactants may noticeably change the phenomena of heat transfer by boiling and convection [31, 32]. Although the literature in this field includes experimental studies in which nanofluids have been used with surfactants to improve nanoparticle dispersion, they have not taken into account the effect of the surfactant on the performance and capillary limit of heat pipes. This study was divided into two stages: first, the stability of several

nanofluids was evaluated using conventional methods (UV–Vis absorbance and visual inspection); and, second, six nanofluids were selected for experimental evaluation.

Materials and methods

Experimental setup

Alumina (Al_2O_3) nanoparticles supplied by Sigma-Aldrich Pty. Ltd (Purity: 99.8% based on trace metals analysis) were used to prepare the nanofluids. Nanoparticles were observed to have sizes in the range between 12 and 50 nm approximately. Deionized (DI < 18.2 MΩ cm resistivity) water/Al_2O_3-based nanofluids were produced with concentrations of 0.1 mass/%, 0.5 mass/%, and 1.0 mass/%. Anionic surfactant sodium dodecylbenzene sulfonate (SDBS in chemical grade, Sigma-Aldrich Pty. Ltd.) was selected as dispersing agent in two mass percentages: 0.064 mass/% and 0.32 mass/%. Nanofluids preparation and stability have been previously investigated and carried out by the authors [33] employing a 3^2 random experimental design with two replicates, as shown in Table 1. Thus, the nanofluids with the highest temporal stability and one unstable dispersion (detailed in Table 2) were selected for heat pipe tests.

Figure 1 shows the average hydrodynamic size of the Al_2O_3 dispersed in water after the nanofluid preparation, which was obtained with the dynamic light scattering technique (DLS) at a Zetasizer Nano ZS (Malvern Instruments Inc., UK); Average sizes were between 196 and 241 nm, except the nanofluid with a Al_2O_3 concentration of 0.5 mass% and SDBS 0.064 mass%, this result could be attributed to high agglomeration rate and sedimentation of the particles [33]

In other hand Fig. 2 presents the experimental setup employed in this study. It consists of a copper heat pipe with inner and outer diameters of 9.525×10^{-3} m and 12.7×10^{-3} m, respectively, and a length of 0.44 m. The cooling system comprises a nylon water jacket, with an inner diameter of 70×10^{-3} m and a length of 0.2 m, which is connected to a container filled with water cooled by a circulating thermostatic bath (TC-502, Brookfield) to maintain a constant temperature of 23 ± 1.4 °C at the jacket inlet with a mass rate of 0.0298 ± 0.0011 kg s^{-1}. The heating system includes an electrical coil wrapped around 0.15 m of the evaporator section, which is controlled by two DC power supply units (BK 1672, TEquiment LLC Company, USA) connected in series. The evaporator and adiabatic zone are covered with fiber glass and Rubaflex insulation.

Table 1 Experimental design of the nanofluids preparation

Experimental design			
Factor	Experimental domain		
	Low level	Middle level	High level
Al_2O_3 concentration	0.1 mass/%	0.500 mass/%	1.00 mass/%
SDBS concentration	0.0 mass/%	0.064 mass/%	0.32 mass/%

Table 2 Nanofluids for heat pipe tests

Nanofluid preparation order	Nanofluid designation	Al_2O_3 concentration/mass/%	SDBS concentration/mass/%
1	NF-1	0.1	0.064
2	NF-2	0.1	–
3	NF-3	0.5	0.320
4	NF-4	0.1	0.320
5	NF-5	0.5	–
6	NF-6	1.0	–
7	NF-7	0.5	0.064

A data acquisition system (DAQ 5203) was directly connected to twelve T-type thermocouples located along the heat pipe, as shown in Fig. 3a. Thermocouples T1 to T7 were placed in the evaporator; T8 and T9, in the adiabatic zone; and T10 to T12, attached to the condenser. Heat pipe tests were conducted in the horizontal position, and a stainless-steel mesh with 200 openings per inch was used as capillary material. Such mesh was installed inside the tube, ensuring that it covered three turns and it was in full contact with the inner walls of the tube (Fig. 3a and Fig. 3b).

Experimental procedure

A vacuum pressure of − 74,500.6 Pa was applied to the heat pipe using a vacuum pump (ME 1C, VACUUMBRAND) with the aim of removing non-condensable gases (NCG) inside it and avoiding the thermal resistance associated with them. Subsequently, the heat pipe was filled with the quantity of fluid necessary to saturate the porous medium, which was calculated using Eqs. (1) to (5) [34, 35]. Porosity (ε) was calculated using Eq. (1).

$$\varepsilon = 1 - \frac{1.05\pi \cdot N \cdot d_c}{4} \quad (1)$$

where N and d_c are the number of openings per lineal meter and the thread diameter, respectively. The mesh number was 7936 m^{-1} (#200), and Fig. 4 shows the diameter of the thread, i.e., $4.6 \times 10^{-5} \pm 1.3$ m, a value close to the 5×10^{-5} m mentioned by the ESDU [34].

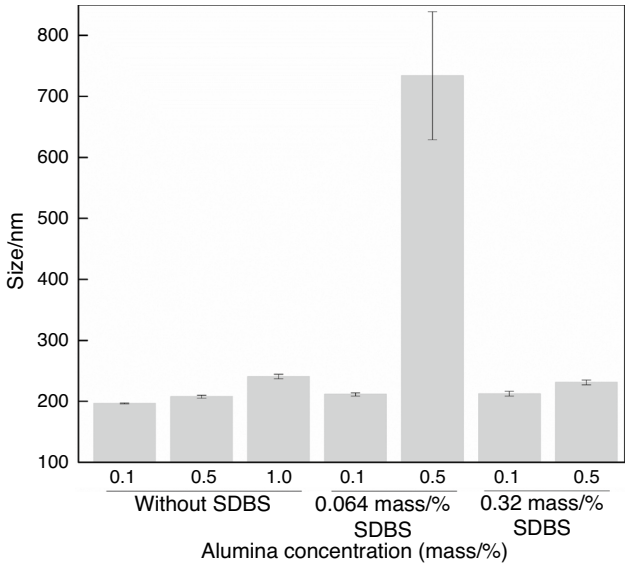

Fig. 1 Particles size distribution measurement based in the DLS of each nanofluid

$$V_c = \left(\frac{\pi}{4} \cdot \varnothing_{in}{}^2 - \pi \cdot r_v{}^2\right) \cdot h \tag{4}$$

where the heat pipe height (h) was 0.44 m. Finally, the overall volume of the voids in the mesh was calculated by solving Eq. (5) and using porosity.

$$V_{t,c} = V_c \cdot \varepsilon \tag{5}$$

The quantity of fluid necessary to fill the system was estimated at 4.0 X 10^{-6} m^3. Additionally, an excess of 10% was added in order to avoid an early dry-out of the mesh. Therefore, the amount of water or nanofluid used in each test was 4.4 X 10^{-6} m^3. The filling process was carried out in four steps, as shown in Fig. 5: (1) water or a nanofluid was poured into a burette to measure its volume, (2) the burette was attached to the heat pipe using low-porosity hoses and a pneumatic fitting, (3) surgical forceps were used to avoid air infiltrations into the pipe, and (4) the burette valve was opened.

While the fluid filled the low-porosity hoses located above the surgical clamps, a vacuum pump was used to remove air bubbles present in both the fluid and the hoses; this procedure avoids non-condensable gases (NCG). Finally, the surgical forceps were opened and then closed when the exact volume of fluid had filled the heat pipe.

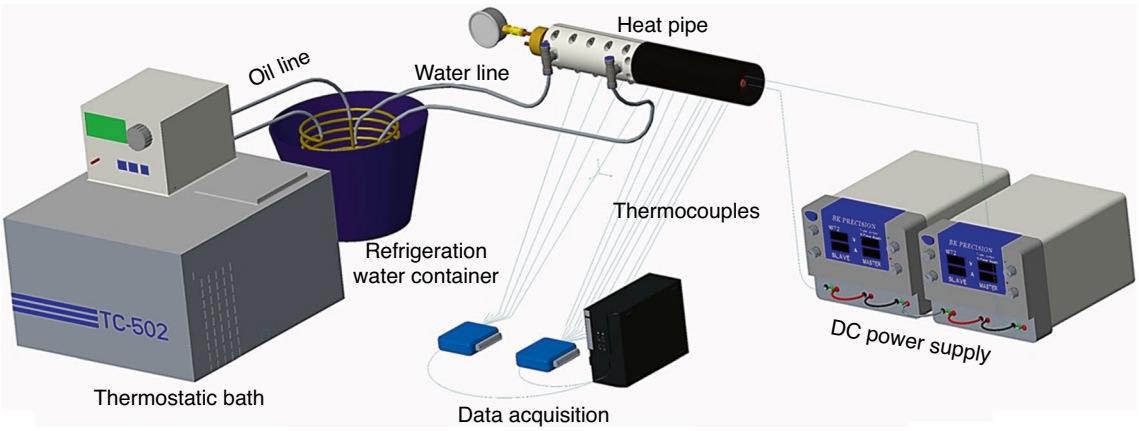

Fig. 2 Schematic diagram of the experimental setup

Likewise, the permeability (K) was calculated by solving Eq. (2) [34].

$$K = \frac{d_c{}^2 \cdot \varepsilon^3}{122 \cdot (1-\varepsilon)^2} \tag{2}$$

The vapor-core radius (r_v) was given by Eq. (3).

$$r_v = \frac{\varnothing_{in} - 4(e \cdot Turnofthemesh)}{2} \tag{3}$$

where $\varnothing_{in}$ is the inner diameter of the heat pipe and e is the mesh thickness, with a value of 8×10^{-5} m. The mesh volume can be obtained using Eq. (4).

Heat was applied using a variable resistance heater with a variation of the input power controlled by the DC power supply. The amount of applied power was increased by 5 W every half an hour until the capillary limit was reached, which was evident when the evaporator section overheated due to the dry-out phenomenon because the liquid fluid was unable to return from the condenser to the evaporator as a result of pressure losses.

The presence of NCG was not considered in the assessments because the experimental data of each replica showed

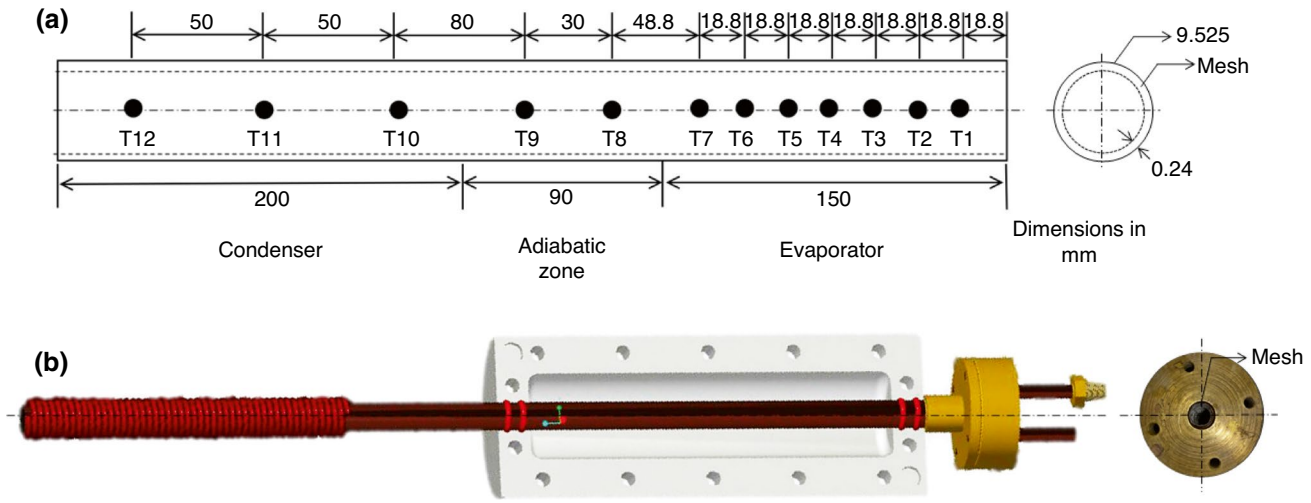

Fig. 3 Distribution of thermocouples along the heat pipe **a** and mesh positioning **b**

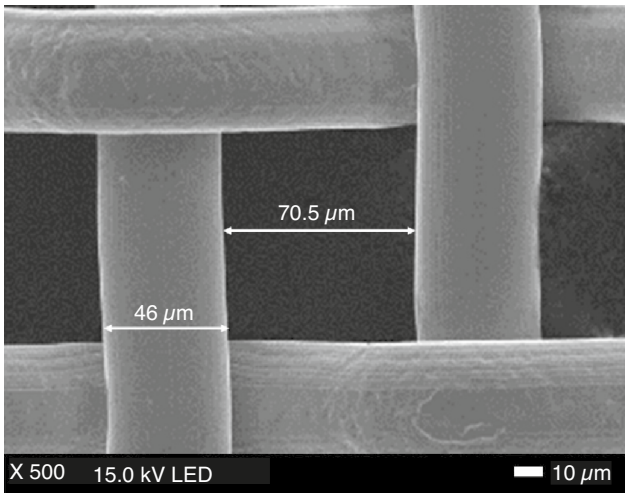

Fig. 4 FE-SEM image of the screen mesh size

no statistically significant difference. Additionally, Reay and P. Kew [35] have indicated that copper–water tests in heat pipes could be conducted over long periods (more than 20,000 h) at low temperatures without degradation or NCG generation, and stainless steel-water tests could generate NCG only after long periods of time.

After the heat pipe tests, the deposition and roughness of the nanoparticles were measured using a FE-SEM and an atomic force microscopy (AFM), respectively. An AFM can continuously track the topography of a surface or sample. In this paper, an AFM (Park systems–NX20 300 mm) was used in order to investigate changes on the surface of the meshes after operating inside the heat pipe with each nanofluid. Six different wires of each mesh were analyzed over an area of 8×10^{-6} m X 8×10^{-6} m at a scan rate of 1.5 Hz.

The overall thermal resistance, R, of the heat pipe was calculated using Eq. (6).

$$\boldsymbol{R} = \frac{\overline{\boldsymbol{T}_e} - \overline{\boldsymbol{T}_c}}{\dot{\boldsymbol{Q}}_{in}} \tag{6}$$

where $\overline{T_e}$ and $\overline{T_c}$ are the average temperatures of the evaporator (T1–T7) and the condenser sections (T0–T12), respectively, and $\dot{Q}_{in}$ denotes the heat input controlled by the DC power supply. In addition, the heat transfer coefficient was calculated by solving Eq. (7).

$$\boldsymbol{h}_e = \frac{\dot{\boldsymbol{Q}}_{in}}{\boldsymbol{A}_e \Delta \boldsymbol{T}_e} \tag{7}$$

where h_e is the heat transfer coefficient and A_e is the evaporator's heat transfer area. The temperature difference in the evaporator (ΔT_e) was calculated using Eq. (8).

$$\Delta \boldsymbol{T}_e = \boldsymbol{T}_e - \boldsymbol{T}_v \tag{8}$$

where T_v is the temperature of the saturated vapor (equal to the temperature in the adiabatic zone). Additionally, the uncertainty of the experimental results was calculated using the manufacturer's specifications of each device. Equations (9), (10), and (11) are implemented to calculate the uncertainty of the heat input, temperature difference, and overall thermal resistance, respectively [11]:

$$\frac{\Delta \boldsymbol{Q}}{\boldsymbol{Q}} = \sqrt{\left(\frac{\Delta \boldsymbol{V}}{\boldsymbol{V}}\right)^2 + \left(\frac{\Delta \boldsymbol{I}}{\boldsymbol{I}}\right)^2} \tag{9}$$

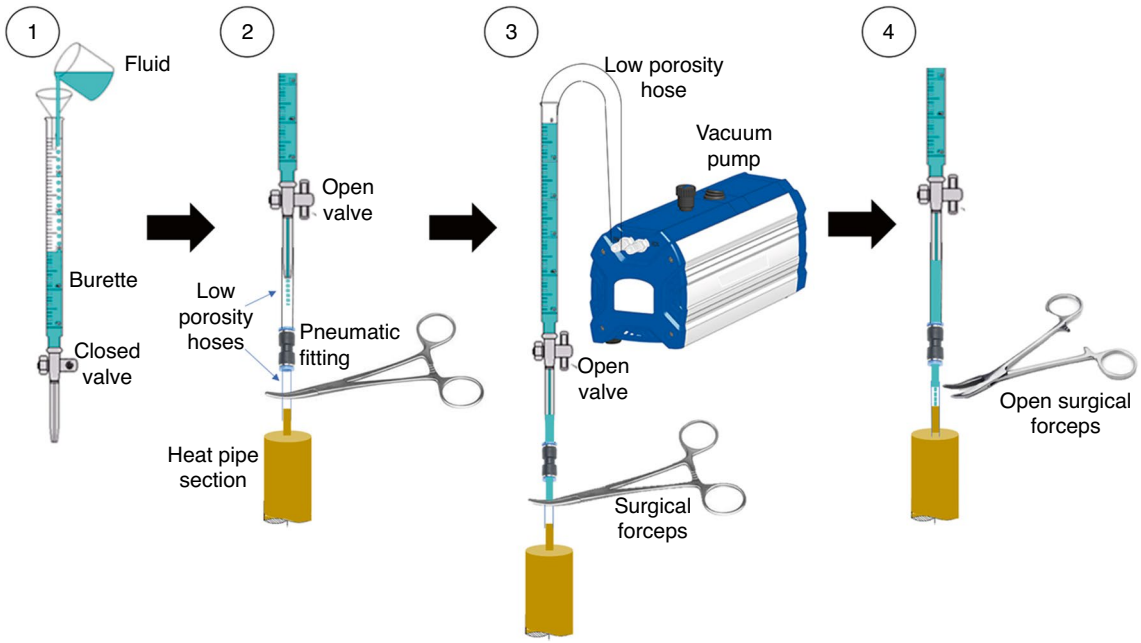

Fig. 5 Heat pipe filling procedure

Table 3 Associated uncertainty of some experimental variables

Variable	Associated uncertainty
Thermocouples	±0.3 K
Heat pipe input	±0.6%
Temperature difference	±3.7%
Thermal resistance	±0.61%
Mass flow	±0.0011 kg s^{-1}

$$\Delta T = \sqrt{\left(\frac{\delta\Delta\overline{T}_e}{\delta\overline{T}_e}\Delta\overline{T}_e\right)^2 + \left(\frac{\delta\Delta\overline{T}_c}{\delta\overline{T}_c}\Delta\overline{T}_c\right)^2} \tag{10}$$

$$\frac{\Delta R}{R} = \sqrt{\left(\frac{\Delta Q}{Q}\right)^2 + \left(\frac{\Delta(\Delta T)}{\Delta T}\right)^2} \tag{11}$$

Table 3 shows several uncertainty values that were calculated. Furthermore, mass flow uncertainty was obtained by means of the immersion pump flow and the difference between the measurements in 0.1 L and 0.05 L test tubes.

Results and discussion

Thermal performance and capillary limit of the heat pipe

On the one hand, Fig. 6 details the change in thermal resistance of the heat pipe caused by input power variations. The thermal resistance clearly represents the thermal performance of the heat pipe and the points where the capillary limit appears for each nanofluid used as working fluid. The operation limit was detected when the thermal resistance at the evaporator exhibited a sudden increase, as a result of a dry-out in the evaporator. These circumstances did not allow the heat pipe to achieve a steady state after the power change, which represents high thermal resistance and high uncertainty in the results. At that point, the test was considered finished, and, for that reason, many of the points (nanofluids) in the figure are shown only up to low power levels.

Using Al_2O_3 nanofluids at 0.1 mass/%, 0.5 mass/%, and 1.0 mass/%, the capillary limits were found at 80 W, 75 W, and 70 W, respectively, as shown in Fig. 6a. Furthermore, each one of those concentrations produced a maximum thermal resistance reduction of 30%, 29%, and 43%, respectively. The general consensus in the literature is that the use of nanoparticles enhances the thermal properties of the base fluids and, thereby, improves the thermal performance and the capillary limit of heat pipes [4, 9]. Such enhancement is attributed to the presence of nanoparticles on the mesh and the heat transfer surface since roughness, nucleation sites, and capillary pumping change in the presence of deposited

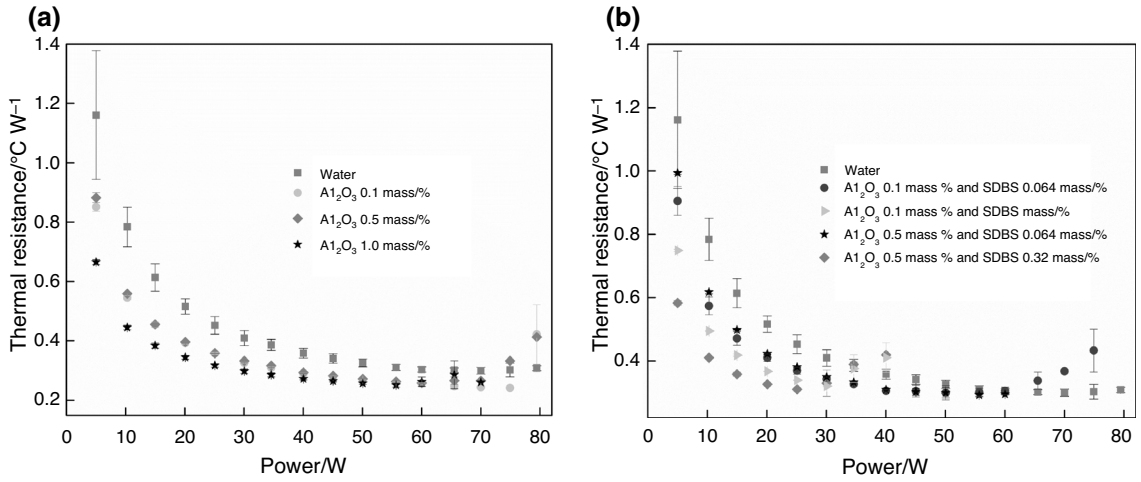

Fig. 6 Change in thermal resistance under different power variations **a** without SDBS and **b** with SDBS

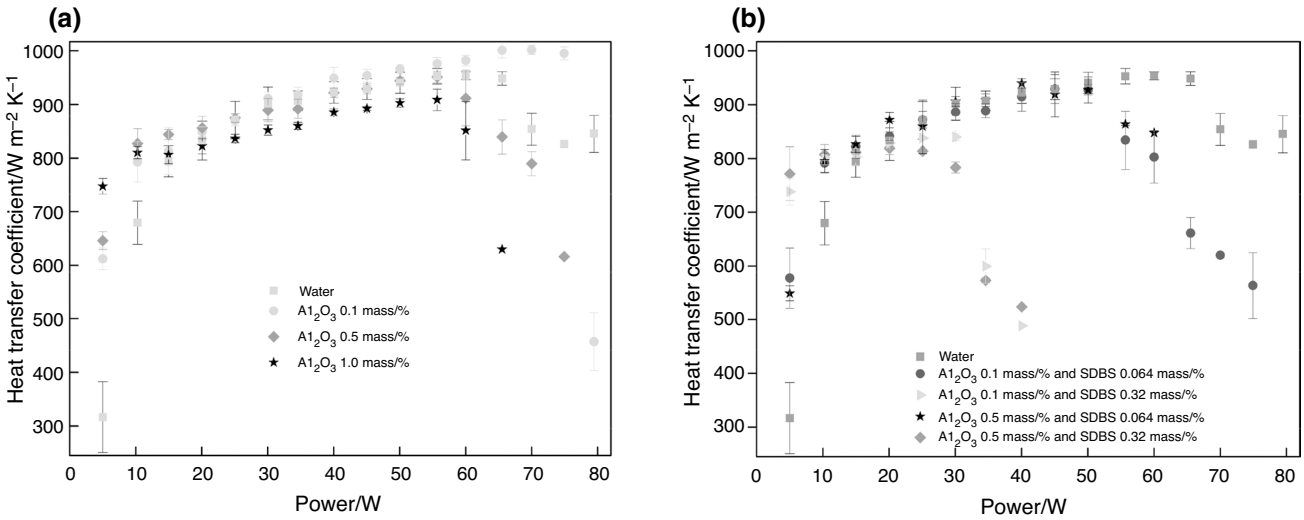

Fig. 7 Heat transfer coefficient under different power variations **a** without SDBS and **b** with SDBS

nanoparticles, which modify the heat transfer mechanism [36]. However, in this study, the capillary limit was affected when the nanoparticle concentration was increased to 0.5 mass/% and 1.0 mass/%, which was attributed to the reduction of flow channels due to the obstruction of the capillary mesh by deposited nanoparticles [37].

On the other hand, Fig. 6b shows that the thermal resistance of the heat pipe was consistently reduced when SDBS was added to the nanofluids, and the combination that produced the highest temporal stability was a 0.5 mass/% concentration of Al_2O_3 and 0.32 mass/% of SDBS. This confirms that stable nanofluids are suitable to be used in heat pipes because longer stability reduces operation uncertainly and guarantees nanofluids with highly dispersed nanoparticles during and after operation. However, this situation is possible only at low power levels (below 25 W), since the capillary limit was reached between 35 and 55 W. This may be due to the reduction in surface tension produced by the presence of surfactant, which deteriorates the operation of the heat pipe by limiting the amount of fluid that is pumped from the condenser to the evaporator by capillarity [38].

Figure 7 shows the heat transfer coefficient (HTC) of the evaporator with respect to the heat flux using water and nanofluids as working fluid. In the interval between 15 and 50 W, there is a statistically negligible difference between each test, except for concentrations of 0.1 mass/% and 0.5 mass/% with 0.32mass/% of SDBS, as shown in Fig. 7b, which are characterized by the presence of a high concentration of surfactant that, as mentioned above, reduces the surface tension of the nanofluid and favors the deterioration of

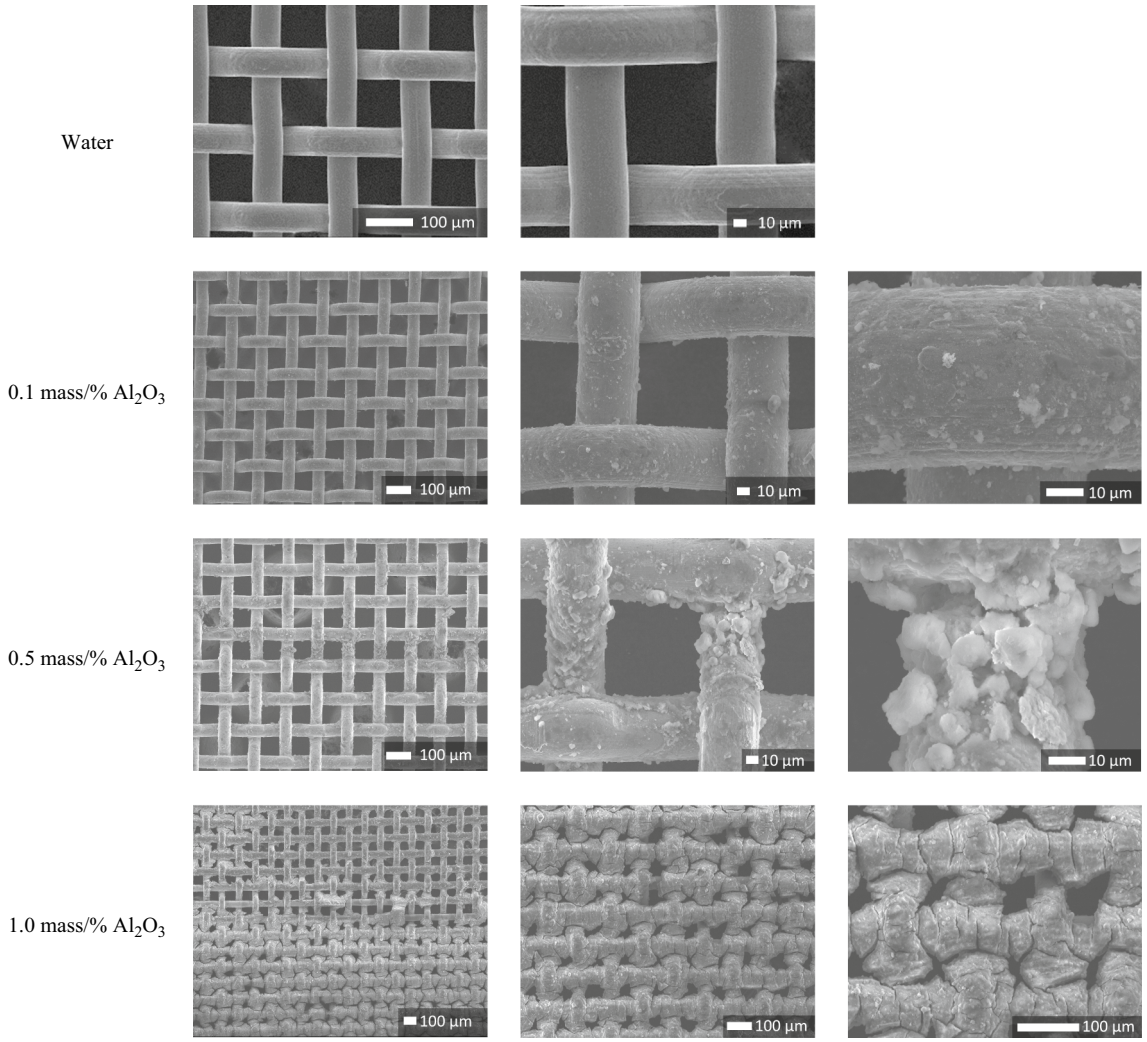

Fig. 8 FE-SEM images of the meshes after the operation with SDBS-free nanofluids

the operation of the heat pipe. The phenomenon associated with the deterioration of the thermal performance can be noticed outside such interval because, when the temperature and thermal resistance increased (as shown in Fig. 6), the HTC decreased [39].

Above 50 W, Fig. 7a shows the best result was produced with a concentration of 0.1 mass/% of nanoparticles and no SDBS; in that case, the HTC was 17% higher than with water. This HTC increase might be caused by changes in the evaporator's surface and the mesh due to the presence of nanoparticles since surface area and roughness increase convection heat transfer mechanisms and capillary pumping capacity [39].

Furthermore, the phenomenon of progressive dry-out of the wick was reduced due to an improvement in wick wettability. Nevertheless, excessive nanoparticle concentrations (e.g., 1.0 mass/%) may reduce the HTC due to large numbers of deposited nanoparticles that create additional thermal resistance caused by clogging of the capillary channels [19, 40, 41].

Analysis of the deposition of nanoparticles on the mesh after operation

Figure 8 shows the FE-SEM image of each screen mesh after the heat pipe tests with the SDBS-free nanofluids. Deposition occurs when nanoparticles come into contact with a surface and due to agglomeration and sedimentation processes, which could improve the heat pipe's performance because capillary pumping may take place due to a reduction of the effective capillary radius [39]. Thus, the deposition of Al_2O_3 nanoparticles and some agglomerates can be observed on the wires of the mesh. Using Al_2O_3 concentrations of 0.1 mass/%, a uniform distribution of nanoparticles over the mesh was obtained after the heat pipe operation; this could explain the higher capillary limit compared to water.

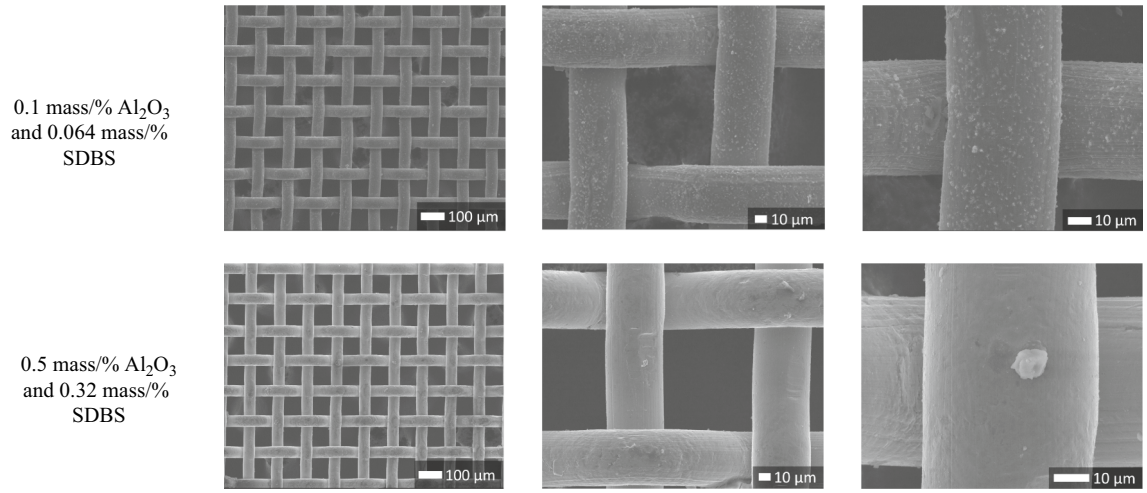

Fig. 9 FE-SEM images of the meshes after the operation with some nanofluids mixed with SDBS

However, large agglomerates and blocked mesh pores were obtained with Al_2O_3 concentrations of 0.5 mass/% and 1.0 mass/%, which prevented the fluid from being pumped from the condenser back to the evaporator. This could explain the early failure of the heat pipe operating with these two concentrations because, at high input powers, vapor production and the return of condensate to the evaporator increase, which could be unbalanced due to blocked pores [19, 37, 42].

Wettability could change with the use of nanofluids because large numbers of nanoparticles on the mesh modify the wetting angle between the mesh and the working fluid. Furthermore, the reduction in wetting angle improves the thermal performance of the heat pipe because the capillary pressure is strongly dependent on the wettability of the fluid on the capillary medium [43]. In previous research, Herrera et al. [44] investigated the wetting angle of water and Al_2O_3 nanofluids at concentrations of 0.1 mass/%, 0.5 mass/%, and 1.0 mass/% over a stainless-steel screen mesh. They found that the wetting angle decreased as the Al_2O_3 nanoparticle concentration increased. Therefore, the deposition of nanoparticles on the mesh surface could improve wettability and capillary limit because the maximum capillary pumping is directly proportional to the wettability of the working fluid; however, large numbers of deposited nanoparticles deteriorate wettability and wetting angles increase.

In this study, an Al_2O_3 concentration of 0.5 mass/%, an SDBS concentration of 0.32 mass/%, and input powers lower than 25 W produced a lower thermal resistance than water because, under that operating regime, there is a better wettability of the mesh, which improves the heat transfer area and the convection heat transfer mechanism, increasing the velocity of the fluid's return from the condenser to the evaporator [11]. Similarly, the use of surfactant improved the reproducibility of the nanofluid tests at low input powers because there was a better dispersion of the particles deposited on the mesh, which prevented the formation of large agglomerates that can block the pores of the capillary medium, as shown in Fig. 9.

In order to verify the findings above, the wetting angle of the Al_2O_3-SDBS nanofluids was measured employing a Drop Shape Analyzer (DSA25E–Krüss Inc.), and a sample of a stainless-steel screen mesh was used as contact surface. The results shown that SDBS becomes completely hydrophilic on the sample mesh, as opposed to water and SDBS-free nanofluids. Additionally, when the concentration of surfactant (SDBS) was 0.32 mass/%, the mesh became wet faster than when using 0.064 mass/% because the nanofluid was distributed over the entire sample mesh in 1.57 s and 0.57 s with nanoparticle concentrations of 0.1 mass/% and 0.5 mass/%, respectively. With SDBS and Al_2O_3 concentrations of 0.064 mass/% and 0.1 mass/%, respectively, the time it took the mesh to be completely wet was 4.24 s. Thus, nanofluid wettability was improved with high concentrations of both Al_2O_3 and SDBS. This is due, first, to the reduction of wetting angle with the use of nanoparticles and, second, to the moisturizing property of the surfactant because, by reducing the surface tension of the nanofluid, the attraction of the fluid to the surface of the mesh is promoted through the mechanism of polar attraction [45].

Roughness analysis of meshes after heat pipe operation

Figure 10 shows the roughness of each mesh after the operation with nanofluids. Roughness can be obtained as two different indicators, i.e., Ra and Rq, which are both used to calculate surface roughness through the measurement of

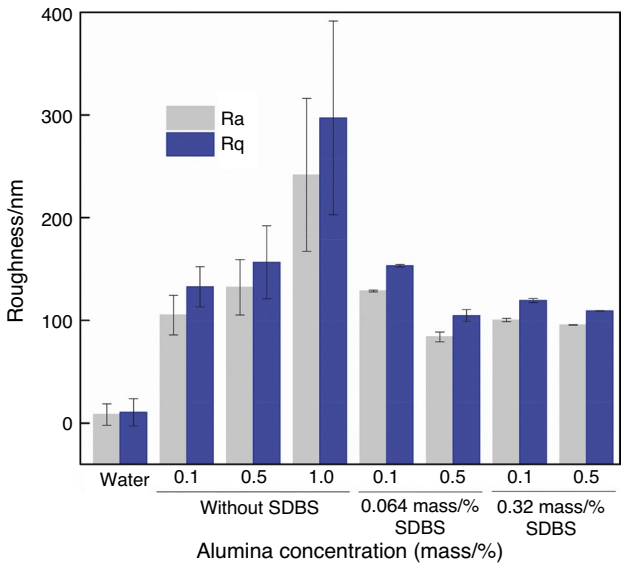

Fig. 10 Roughness results of each mesh after the heat pipe operation with the nanofluids

microscopic peaks and valleys. However, Ra is calculated as the mean arithmetic deviation; and Rq, as the root mean square.

The results show that the nanofluids with Al_2O_3 concentrations of 0.1 mass/%, 0.5 mass/%, and 1.0 mass/% (NF-2, NF-5, and NF-6, respectively) significantly increase the roughness of the meshes compared to water. Additionally, the distribution of nanoparticles over the meshes was non-uniform, as indicated by the error bars and confirmed in the FE-SEM images in Fig. 8. The results obtained with Al_2O_3 concentrations of 0.1 mass/% and 0.5 mass/% may be affected by the non-uniformity of the nanoparticle distribution, and this might be the reason why the roughness results are apparently similar in spite of the fact that the FE-SEM images confirm the presence of large agglomerations when an Al_2O_3 concentration of 0.5 mass/% was employed. However, because of that similar roughness, the thermal performance values of the two concentrations were close to each other in the range from 10 to 60 W, as shown in Fig. 6. After 60 W, large agglomerations in the mesh reduced the capillary capacity in the heat pipe when an Al_2O_3 concentration of 0.5 mass/% was used, as show in the FE-SEM images in Fig. 8. A similar result was found by Kole and Dey [36] and Ghanbarpour et al. [11], that is, deposited nanoparticles can improve surface wettability, surface roughness, and capillary action; however, a layer of aggregated and agglomerated nanoparticles negatively affects the surface roughness and heat transfer mechanism by reducing the wettability and blocking mesh pores.

The SDBS improved the distribution of the nanoparticles over the meshes, as shown in Figs. 9 and 10. Said surfactant also helped to enhance the temporal stability of the nanofluids, as confirmed by the absorbance analysis of Al_2O_3 and SDBS at concentrations of 0.5 mass/% and 0.32 mass/% (NF-3), respectively. During the operation, the use of SDBS promoted the distribution of nanoparticles over the mesh because the nanofluids presented improved wettability and nanoparticle deposition with respect to nanofluids with Al_2O_3 only; this is due to the polar attraction mechanism mentioned above. Nonetheless, the use of surfactant decreases surface tension. Therefore, in this study, the use of surfactant improved the heat pipe's performance until 40 W, but it reduced the capillary capacity of the mesh because of the surface tension decrease.

Figure 11 shows the 3D roughness plots of the results. The values of the mesh used in tests with water are close to 0 nm. In turn, the mesh that was in contact with Al_2O_3 nanoparticles (0.1 mass/%, 0.5 mass/%, and 1.0 mass/%) presents high agglomerations, specially at an Al_2O_3 concentration of 1.0 mass/%; for that reason, the AFM analysis revealed a thick and uniform layer. However, with the use of SDBS, after the operation, the meshes exhibit a high distribution of nanoparticles; thus, more peaks and valleys are formed, which confirms the results above and increases the heat transfer surface.

Influence of surface tension on capillary limit and thermal performance

Figure 12 presents the surface tension results of water and the nanofluids. In order to separately analyze the effects that nanoparticles and surfactant have on this property, SDBS-water mixtures prepared at surfactant concentrations of 0.064 mass/% and 0.32 mass/% were also measured. Compared to DI-water, Al_2O_3 concentrations of 0.1 mass/%, 0.5 mass/%, and 1.0 mass/% caused surface tension increases of 10%, 9%, and 12%, respectively. Such increases could be explained by the fact that van der Waals forces between particles at the liquid–gas interface could increase surface free energy, leading to higher surface tension.

However, some conflicting surface tension results have been reported in the literature [46]. While some authors have shown that surface tension increases with the addition of nanoparticles [47, 48], others have found the opposite behavior, even in nanofluids based on the same fluid and nanoparticle type [49].

In this study, the increase in surface tension could also explain the improved capillary pumping capacity produced by an Al_2O_3 nanoparticle concentration of 0.1 mass/% because the capillary pumping pressure is a physical variable that depends directly on surface tension, and it is inversely proportional to the effective capillary radius. Therefore, when surface tension rises and the effective capillary radius

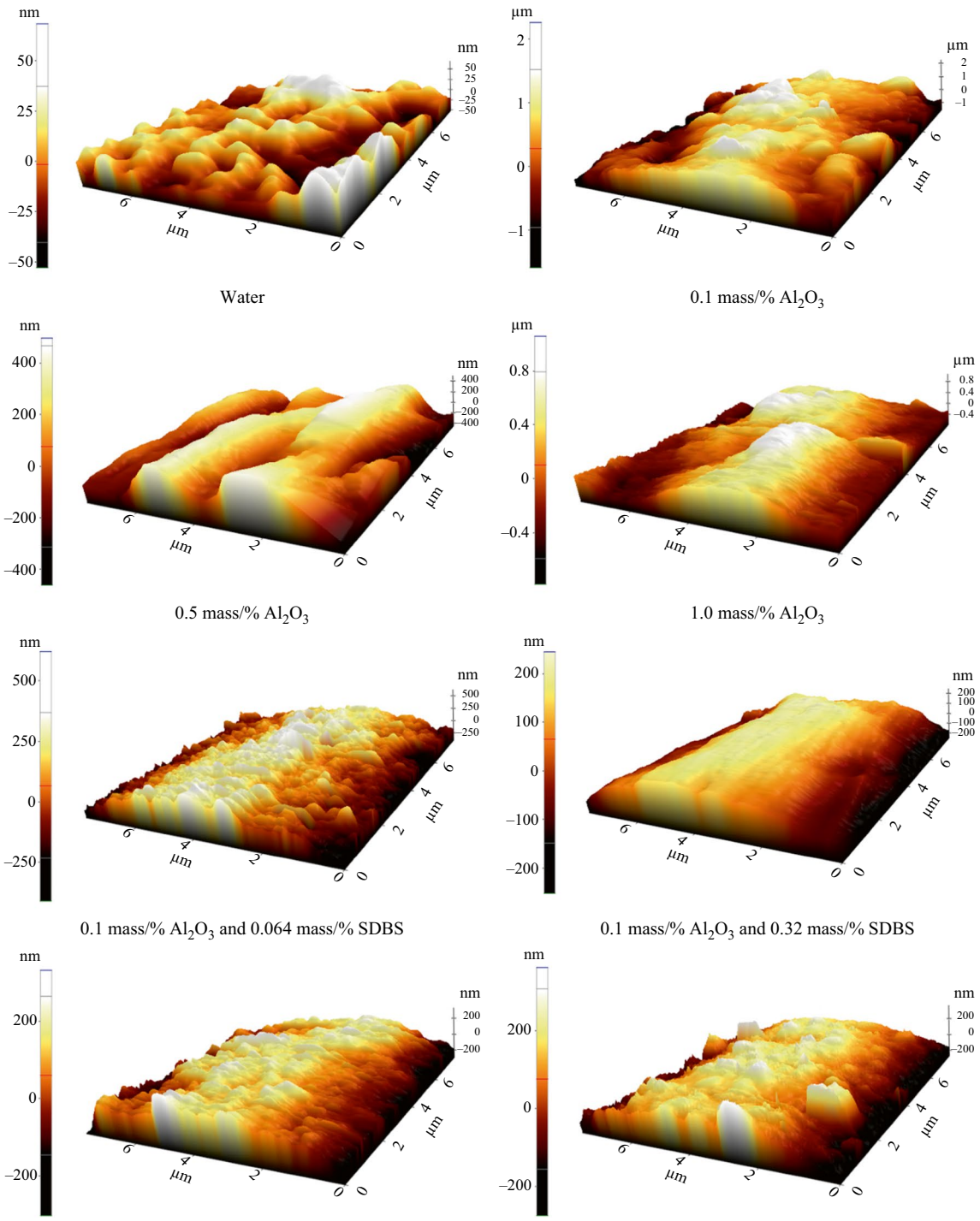

Fig. 11 3D roughness plots of the AFM images of each mesh after the heat pipe operation with nanofluids

is reduced due to the deposition of nanoparticles on the mesh wires, the capillary limit is improved, as show in Fig. 8.

During the tests with Al_2O_3 concentrations of 0.5 mass/% and 1.0 mass/%, the capillary limit was reached earlier than with water despite exhibiting increases in surface tension as a result of the presence of large agglomerates of nanoparticles and blockages of flow channels due to the high concentration of nanoparticles, as shown in Fig. 8. However, the effect of surfactant concentration becomes more important than that of nanoparticle concentration when the surface tension of nanofluids is measured. Thus, nanofluids with Al_2O_3 concentrations of 0.1 mass/% and 0.5 mass/% and an

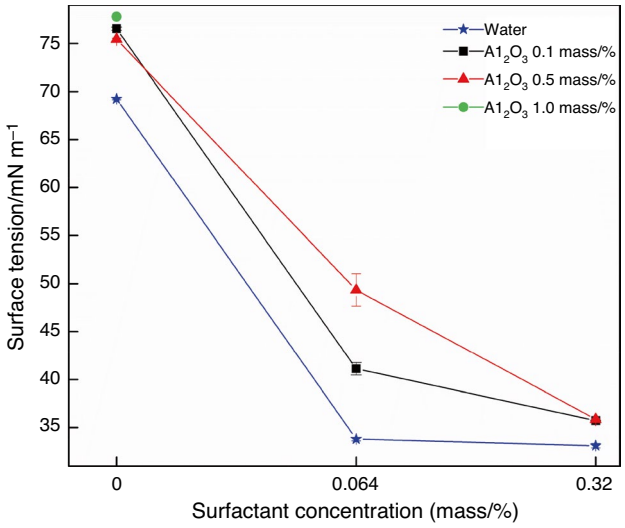

Fig. 12 Surface tension of Al_2O_3-based nanofluids

SDBS concentration of 0.064 mass/% presented surface tension reductions of approximately 41% and 29%, respectively, compared to water. Nevertheless, the surface tension of the nanofluid with 0.5 mass/% Al_2O_3 and 0.064 mass/% SDBS, which was described above as the most unstable nanofluid, exhibited a high uncertainty with respect to the recommendation provided by the manufacturer of the tensiometer (deviation under 0.1 mN m^{-1}).

The Al_2O_3 nanofluids at 0.1 mass/% and 0.5 mass/% and SDBS at 0.32 mass/% reduced the surface tension by approximately 48% compared to DI-water. This result is consistent with those reported in the literature since surfactants reduce the surface tension of the base fluid between 50 and 70% [49, 50]. In this study, the heat pipe tests presented problems at high input powers using nanofluids with surfactant, mainly with SDBS at 0.32 mass/%. This occurred because of the reduction in capillary pumping caused by a surface tension decrease; therefore, the amount of condensed fluid that returns from the condenser to the evaporator is unbalanced and the nanofluids with SDBS reach their capillary limit earlier. In this experiment, the use of SDBS and Al_2O_3 concentrations of 0.1 mass/%, 0.5 mass/%, and 1.0 mass/% enabled an improvement in the thermal performance of the heat pipe at a power input of 40 W with respect to water. However, above 40 W, the heat pipe was unable to operate normally due to the capillary limit.

Conclusions

This study experimentally evaluated the thermal performance and capillary limit of a heat pipe using nanofluids with alumina nanoparticles and SDBS as dispersion method. According to the results, the following conclusions can be drawn:

The capillary limit of the heat pipe using nanofluids with nanoparticles at a concentration of 0.1 mass/% and no SDBS was higher than using water. Additionally, the thermal performance of the heat pipe improved as nanoparticle concentration increased, which was attributed to the increased surface tension, wettability, and roughness generated by the presence of nanoparticles in the fluid and their deposition on the capillary mesh and heat transfer surface. However, high nanoparticle concentrations produce an adverse effect because the pores of the wick are blocked, which prevents the return of fluid from the condenser to the evaporator.

In this case, the use of surfactant caused reductions in surface tension; therefore, when it was added to the fluid, the heat pipe reached its capillary limit faster than when water or SDBS-free nanofluids were employed. The heat pipe achieved its best thermal performance below 25 W using the nanofluid with 0.5 mass/% Al_2O_3 and 0.32 mass/% SDBS (the most stable nanofluid) since it improved properties such as nanoparticle distribution on the meshes, wettability, and roughness.

Acknowledgements The authors gratefully acknowledge the financial support provided by COLCIENCIAS (1118-669-46092 CTO: 126-2015), Instituto Tecnológico Metropolitano (ITM) and, Institución Universitaria Pascual Bravo in Medellín, Colombia.

Authors' contributions AG contributed writing—original draft preparation, investigation, data curation, formal analysis, and methodology. KC contributed conceptualization, project administration, supervision, methodology, investigation, and validation. BH contributed methodology, writing—review and editing, formal analysis, and project administration.

Declarations

Conflicts of interest The authors have no conflicts of interest to declare that are relevant to the content of this article.

References

1. CW Chan, E Siqueiros, J LingChin, M Royapoor, and P Roskilly. Heat utilisation technologies: A critical review of heat pipes. Renew Sustain Energy Rev 2015;50:615–627.
2. Wu Y, Jia J, Tian D, Chuah YK. Heat Transfer Performance of Microgroove Back Plate Heat Pipes with Working Fluid and Heating Power. J Therm Sci. 2020;29(4):982–91. https://doi.org/10.1007/s11630-020-1336-9.

3. Cardin N, Lips S, Siedel S, Davoust L, Bonjour J. Two-phase electrohydrodynamics along a grooved flat heat pipe. Exp Fluids. 2020;61(8):170. https://doi.org/10.1007/s00348-020-03002-9.
4. Poplaski LM, Benn SP, Faghri A. Thermal performance of heat pipes using nanofluids. Int J Heat Mass Transf. 2017;107:358–71. https://doi.org/10.1016/j.ijheatmasstransfer.2016.10.111.
5. Shi C, Wang Y, Liao Q, Yang Y. Analysis and application of variable conductance heat pipe air preheater. J Therm Sci. 2011;20(3):248–53. https://doi.org/10.1007/s11630-011-0466-5.
6. Srimuang W, Amatachaya P. A review of the applications of heat pipe heat exchangers for heat recovery. Renew Sustain Energy Rev. 2012;16(6):4303–15. https://doi.org/10.1016/j.rser.2012.03.030.
7. Hu C, Jia L. Experimental study on the start up performance of flat plate pulsating heat pipe. J Therm Sci. 2011;20(2):150–4. https://doi.org/10.1007/s11630-011-0450-0.
8. Jafari D, Franco A, Filippeschi S, Di Marco P. Two-phase closed thermosyphons: A review of studies and solar applications. Renew Sustain Energy Rev. 2016;53:575–93. https://doi.org/10.1016/j.rser.2015.09.002.
9. Kim KM, Bang IC. Effects of graphene oxide nanofluids on heat pipe performance and capillary limits. Int J Therm Sci. 2016;100:346–56. https://doi.org/10.1016/j.ijthermalsci.2015.10.015.
10. Bertoldo Junior J, Vlassov VV, Genaro G, and Guedes UTV Dynamic test method to determine the capillary limit of axially grooved heat pipes. Exp Therm Fluid Sci. 2015;60:290–8.
11. Ghanbarpour M, Nikkam N, Khodabandeh R, Toprak MS, Muhammed M. Thermal performance of screen mesh heat pipe with Al2O3 nanofluid. Exp Therm Fluid Sci. 2015;66:213–20. https://doi.org/10.1016/j.expthermflusci.2015.03.024.
12. Okonkwo EC, Wole-Osho I, Almanassra IW, Abdullatif YM, Al-Ansari T. An updated review of nanofluids in various heat transfer devices. J Therm Anal Calorim. 2020. https://doi.org/10.1007/s10973-020-09760-2.
13. Buschmann MH. Nanofluids in thermosyphons and heat pipes: Overview of recent experiments and modelling approaches. Int J Therm Sci. 2013;72:1–17. https://doi.org/10.1016/j.ijthermalsci.2013.04.024.
14. Choi SUS. Enhancing thermal conductivity of fluids with nanoparticles. ASME-Publications-Fed. 1995;231:99–106.
15. Yang L, Ji W, Mao M, Huang J. Dynamic stability, sedimentation, and time-dependent heat transfer characteristics of TiO2 and CNT nanofluids. J Therm Anal Calorim. 2020;141(3):1183–95. https://doi.org/10.1007/s10973-019-09103-w.
16. Brahim T, Jemni A. Numerical case study of packed sphere wicked heat pipe using Al_2O_3 and CuO based water nanofluid. Case Stud Therm Eng. 2016;8:311–21. https://doi.org/10.1016/j.csite.2016.09.002.
17. Hassan H, Harmand S. Effect of using nanofluids on the performance of rotating heat pipe. Appl Math Model. 2015;39(15):4445–62. https://doi.org/10.1016/j.apm.2014.12.023.
18. Kamyar A, Ong KS, Saidur R. Effects of nanofluids on heat transfer characteristics of a two-phase closed thermosyphon. Int J Heat Mass Transf. 2013;65:610–8. https://doi.org/10.1016/j.ijheatmasstransfer.2013.06.046.
19. Putra N, Septiadi WN, Rahman H, Irwansyah R. Thermal performance of screen mesh wick heat pipes with nanofluids. Exp Therm Fluid Sci. 2012;40:10–7. https://doi.org/10.1016/j.expthermflusci.2012.01.007.
20. Ghanbarpour M, Nikkam N, Khodabandeh R, Toprak MS. Improvement of heat transfer characteristics of cylindrical heat pipe by using SiC nanofluids. Appl Therm Eng. 2015;90:127–35. https://doi.org/10.1016/j.applthermaleng.2015.07.004.
21. Ghanbarpour M, Nikkam N, Khodabandeh R, Toprak MS. Thermal performance of inclined screen mesh heat pipes using silver nanofluids. Int Commun Heat Mass Transf. 2015;67:14–20. https://doi.org/10.1016/j.icheatmasstransfer.2015.06.009.
22. Kim KM, Jeong YS, Kim IG, Bang IC. Comparison of thermal performances of water-filled, SiC nanofluid-filled and SiC nanoparticles-coated heat pipes. Int J Heat Mass Transf. 2015;88:862–71. https://doi.org/10.1016/j.ijheatmasstransfer.2015.04.108.
23. Arthur O, Karim MA. An investigation into the thermophysical and rheological properties of nanofluids for solar thermal applications. Renew Sustain Energy Rev. 2016;55:739–55. https://doi.org/10.1016/j.rser.2015.10.065.
24. Solangi KH, et al. A comprehensive review of thermo-physical properties and convective heat transfer to nano fl uids. Energy. 2015;89:1065–86. https://doi.org/10.1016/j.energy.2015.06.105.
25. Kamatchi R, Venkatachalapathy S. Parametric study of pool boiling heat transfer with nanofluids for the enhancement of critical heat flux: A review. Int J Therm Sci. 2015;87:228–40. https://doi.org/10.1155/2012/435873.
26. Sureshkumar R, Mohideen ST, Nethaji N. Heat transfer characteristics of nanofluids in heat pipes: A review. Renew Sustain Energy Rev. 2013;20:397–410. https://doi.org/10.1016/j.rser.2012.11.044.
27. Azmi WH, Sharma KV, Sarma PK, Mamat R, Najafi G. Heat transfer and friction factor of water based TiO2 and SiO2 nanofluids under turbulent flow in a tube. Int Commun Heat Mass Transf. 2014;59:30–8. https://doi.org/10.1016/j.icheatmasstransfer.2014.10.007.
28. Chauris N, et al. Experimental investigation of the influence of surfactant on the heat transfer performance of pulsating heat pipe. Appl Therm Eng. 2015;105:364–72.
29. Menlik T, Sözen A, Gürü M, Öztaş S. Heat transfer enhancement using MgO/water nanofluid in heat pipe. J Energy Inst. 2014;88:247–57. https://doi.org/10.1016/j.joei.2014.10.001.
30. Sözen A, et al. A comparative investigation on the effect of fly-ash and alumina nanofluids on the thermal performance of two-phase closed thermo-syphon heat pipes. Appl Therm Eng. 2016;96:330–7. https://doi.org/10.1016/j.applthermaleng.2015.11.038.
31. O. a. Alawi, N. A. C. Sidik, H. a. Mohammed, and S. Syahrullail, "Fluid flow and heat transfer characteristics of nanofluids in heat pipes: A review." *Int Commun Heat Mass Transf*, 2014;56: 50–62.
32. Lee CY, Zhang BJ, Kim KJ. Influence of heated surfaces and fluids on pool boiling heat transfer. Exp Therm Fluid Sci. 2014;59:15–23. https://doi.org/10.1016/j.expthermflusci.2014.07.012.
33. Gallego A, Cacua K, Herrera B, Cabaleiro D, Piñeiro MM, Lugo L. Experimental evaluation of the effect in the stability and thermophysical properties of water-Al2O3 based nanofluids using SDBS as dispersant agent. Adv Powder Technol. 2019. https://doi.org/10.1016/j.apt.2019.11.012.
34. ESDU, "Heat pipes - Performance of capillary-driven design - ESDU 79012," no. September, 1979.
35. D. Reay and P. Kew, "Heat pipe components and materials," *Heat pipes Theory, Des. Appl.*, pp. 108–110, 114, 122, 126–127, 2006,
36. Kole M, Dey TK. Thermal performance of screen mesh wick heat pipes using water-based copper nanofluids. Appl Therm Eng. 2013;50(1):763–70. https://doi.org/10.1016/j.applthermaleng.2012.06.049.
37. Hung Y-H, Teng T-P, Lin B-G. Evaluation of the thermal performance of a heat pipe using alumina nanofluids. Exp Therm Fluid Sci. 2012;44:504–11. https://doi.org/10.1016/j.expthermflusci.2012.08.012.
38. PR Jyothi Sankar. S Venkatachalapathy, LG Asirvatham, and S Wongwises, Effect of coated mesh wick on the performance of cylindrical heat pipe using graphite nanofluids. J Therm Anal Calorim. 2020;146:297–309.

39. Shi C, Wang Y, Xu C. Experimental study and analysis on heat transfer coefficient of radial heat pipe. J Therm Sci. 2010;19(5):425–9. https://doi.org/10.1007/s11630-010-0404-y.
40. Wang PY, Chen XJ, Liu ZH, Liu YP. Application of nanofluid in an inclined mesh wicked heat pipes. Thermochim Acta. 2012;539:100–8. https://doi.org/10.1016/j.tca.2012.04.011.
41. A. B. Solomon, K. Ramachandran, and B. C. Pillai, "Thermal performance of a heat pipe with nanoparticles coated wick," *Appl. Therm. Eng.*, vol. 36, no. 1, pp. 106–112, 2012, doi: https://doi.org/10.1016/j.applthermaleng.2011.12.004.
42. Kumaresan G, Venkatachalapathy S, Asirvatham LG. Experimental investigation on enhancement in thermal characteristics of sintered wick heat pipe using CuO nanofluids. Int J Heat Mass Transf. 2014;72:507–16. https://doi.org/10.1016/j.ijheatmasstransfer.2014.01.029.
43. N. E. Chmielewski, "Design, construction and experimentation of a heat pipe augmented solar wall," University of Louisville, 2008.
44. Herrera B, Chejne F, Mantelli MBH, Mejía J, Cacua K, Gallego A. Population balance for capillary limit modeling in a screen mesh wick heat pipe working with nanofluids. Int J Therm Sci. 2019;138(30):134–58. https://doi.org/10.1016/j.ijthermalsci.2018.12.015.
45. J. Li, B. Du, F. Wang, W. Yao, and S. Yao 2016 "The effect of nanoparticle surfactant polarization on trapping depth of vegetable insulating oil-based nanofluids," *Phys. Lett. Sect. A Gen. At. Solid State Phys.*, 380(4):604–608
46. Estellé P, Cabaleiro D, Żyła G, Lugo L, Murshed SMS. Current trends in surface tension and wetting behavior of nanofluids. Renew Sustain Energy Rev. 2018;94:931–44. https://doi.org/10.1016/j.rser.2018.07.006.
47. Huminic A, Huminic G, Fleaca C, Dumitrache F, Morjan I. Thermal conductivity, viscosity and surface tension of nanofluids based on FeC nanoparticles. Powder Technol. 2015;284:78–84. https://doi.org/10.1016/j.powtec.2015.06.040.
48. Tanvir S, Qiao L. Surface tension of Nanofluid-type fuels containing suspended nanomaterials. Nanoscale Res Lett. 2012;7(1):226. https://doi.org/10.1186/1556-276X-7-226.
49. Khaleduzzaman SS, Mahbubul IM, Shahrul IM, Saidur R. Effect of particle concentration, temperature and surfactant on surface tension of nanofluids. Int Commun Heat Mass Transf. 2013;49:110–4. https://doi.org/10.1016/j.icheatmasstransfer.2013.10.010.
50. Hetsroni G, Zakin JL, Lin Z, Mosyak A, Pancallo E, Rozenblit R. The effect of surfactants on bubble growth, wall thermal patterns and heat transfer in pool boiling. Int J Heat Mass Transf. 2001;44(2):485–97. https://doi.org/10.1016/S0017-9310(00)00099-5.